IMMUNOLOGY

Type 2 immunity induced by bladder extracellular matrix enhances corneal wound healing

Xiaokun Wang[1†], Liam Chung[1,2†], Joshua Hooks[1], David R. Maestas Jr.[1], Andriana Lebid[2], James I. Andorko[1,2], Luai Huleihel[3,4], Alexander F. Chin[1], Matthew Wolf[1,5,6], Nathaniel T. Remlinger[3], Mary Ann Stepp[7], Franck Housseau[2], Jennifer H. Elisseeff[1,2,5]*

The avascular nature of cornea tissue limits its regenerative potential, which may lead to incomplete healing and formation of scars when damaged. Here, we applied micro- and ultrafine porcine urinary bladder matrix (UBM) particulate to promote type 2 immune responses in cornea wounds. Results demonstrated that UBM particulate substantially reduced corneal haze formation as compared to the saline-treated group. Flow cytometry and gene expression analysis showed that UBM particulate suppressed the differentiation of corneal stromal cells into α-smooth muscle actin–positive (αSMA$^+$) myofibroblasts. UBM treatments up-regulated interleukin-4 (IL-4) produced primarily by eosinophils in the wounded corneas and CD4$^+$ T cells in draining lymph nodes, suggesting a cross-talk between local and peripheral immunity. Gata1$^{-/-}$ mice lacking eosinophils did not respond to UBM treatment and had impaired wound healing. In summary, stimulating type 2 immune responses in the wounded cornea can promote proregenerative environments that lead to improved wound healing for vision restoration.

INTRODUCTION

The cornea is the outermost layer of the eye and is therefore susceptible to trauma and injury. Approximately 3% of all emergency department visits are due to eye injury, and most of these involve the cornea (*1*). When corneal transparency is compromised because of injury and the resulting scar formation, keratoplasty is considered to be the most effective therapy to restore vision. Keratoplasty, or cornea transplant, requires donor tissue and surgery with the associated risks and morbidity. New approaches to improve wound healing and reduce scar formation would obviate the need for corneal transplantation. The concept of regenerative immunology and targeting immune cells to improve regeneration is being applied to numerous tissues but has not yet been applied to the cornea.

When the cornea is damaged, injured epithelial cells release cytokines including interleukin 1 (IL-1) and tumor necrosis factor–α (TNF-α), which induce stromal cell apoptosis while simultaneously recruiting immune cells such as neutrophils, macrophages/monocytes, and lymphocytes. These immune cells rapidly infiltrate into the limbal stroma, reaching a peak level around 12 hours with continued inflammation lasting more than 1 week (*2*). These cells produce various cytokines and growth factors such as interleukins and transforming growth factor–β (TGF-β) (*3*). Several cell types reside in healthy corneal stroma including quiescent keratocytes, resident immune cells, and nonmyelinating Schwann cells (*4*). These resident stromal cells are activated by the cytokines and chemokines produced by epithelial cells and immune cells and subsequently proliferate and migrate to the wounded region. At the wound site, they produce extracellular matrix (ECM) to repair the damaged cornea (*5*, *6*). The transition of quiescent stromal cells to myofibroblasts is presumably mediated by TGF-β (*3*, *7*). The overproduction of matrix by myofibroblasts results in an unorganized deposition of ECM proteins such as type III collagen that leads to fibrosis and, eventually, scar formation (*8*). Cross-talk between immune cells recruited to the wounded tissue, activated resident immune cells, and stromal cells controls the delicate balance between regenerative repair that maintains corneal clarity and scar formation that causes loss of vision. Several approaches are currently used to regulate corneal immune responses to reduce corneal scarring, including conventional steroid treatment and cellular therapies to stimulate stromal regeneration (*9*, *10*). Steroids suppress immune responses to decrease inflammation and reduce scar formation following corneal injuries. However, prolonged steroid use results in complications including glaucoma and cataracts (*11*, *12*). Cornea limbal and stromal stem cell therapies have produced promising results in animal models and clinical studies (*13*–*15*). However, the stem cell production and cost may limit large-scale application.

Tissue-derived decellularized ECM is a complex biological biomaterial that includes structural proteins and biological cues that promote tissue repair. Human and porcine ECM manufactured from a variety of tissue sources such as skin, heart, intestine, bladder, and adipose have shown tissue repair efficacy in preclinical models, clinical testing, and commercial use (*16*, *17*). While early studies on ECM scaffolds focused on using the structural cues to promote cell migration and stem cell differentiation, more recent investigations revealed that ECM scaffolds also actively regulate immune responses and create a proregenerative immune environment when implanted to damaged tissue (*18*, *19*). These biomaterials actively participate in immune cell recruitment and activation that help direct the tissue repair process (*20*). For example, Brown *et al.* (*21*) identified proregenerative macrophages that responded to ECM scaffolds and demonstrated that they were required for the scaffolds to promote skeletal muscle regeneration (*22*). In addition to macrophages, the ECM biomaterials required CD4$^+$ T helper type 2 (T_H2) cells and

[1]Translational Tissue Engineering Center, Johns Hopkins School of Medicine, Baltimore, MD 21231, USA. [2]Bloomberg-Kimmel Institute for Cancer Immunotherapy and Sidney Kimmel Comprehensive Cancer Center, Johns Hopkins University School of Medicine, Baltimore, MD 21231, USA. [3]ACell Inc., Columbia, MD 21046, USA. [4]McGowan Institute for Regenerative Medicine, University of Pittsburgh, Pittsburgh, PA 15219, USA. [5]Department of Biomedical Engineering, Johns Hopkins University, Baltimore, MD 21218, USA. [6]Laboratory of Cancer Immunometabolism, Center for Cancer Research, National Cancer Institute, Frederick, MD 21702, USA. [7]Department of Anatomy and Cell Biology and Department of Ophthalmology, School of Medicine and Health Sciences, George Washington University, Washington DC 20037, USA.
*Corresponding author. Email: jhe@jhu.edu
†These authors contributed equally to this work.

IL-4 production to stimulate tissue repair (*23*). Porcine urinary bladder–derived matrix (UBM), a commercially available ECM product, increases the number of IL-4–producing cell populations recruited into wounded tissues (*24*, *25*). The impact of IL-4 and type 2 immune responses on corneal wound healing has not yet been investigated from an immunoengineering standpoint.

While type 2 cell–mediated immunity emerged as a regulator of wound repair in tissues such as muscle and lung (*26*, *27*), there has been minimal application of these therapies in treating corneal wounds and regulating fibrosis in the eye. This gap presents an opportunity to design immunomodulatory therapies to enhance regenerative repair that restores tissue function and, in the cornea, reduce haze formation so that vision is maintained. Our previous study reported that ECM microparticles applied as a wound dressing for injured rabbit corneas reduced the inflammatory reaction and scar formation. However, the underlying mechanism of the immune response to ocular injury and repair was yet to be revealed (*28*). In the current study, we applied different UBM particulate formulations to wounded corneas and investigated the immunological and corneal wound healing responses to the treatment. Results demonstrated that UBM treatment enhanced wound healing and reduced scar formation after injury via IL-4 signaling predominantly from eosinophils in the cornea. Further, UBM particle size could be tuned to modulate the level of this response. Instead of suppressing the immune response to cornea damage via traditional steroid treatment, we use the immune response and direct it toward a desired regenerative phenotype.

RESULTS

UBM treatment reduces corneal scarring

Application of biological ECM scaffolds to the cornea presents a number of challenges including the need to maintain vision and adequate retention in the context of the tear film and fluid flow. We tested formulations of UBM in the ocular environment, including micro- and ultrafine (UF)-scaled-scaled UBM materials.

We first evaluated the physical properties and degradation kinetics of the micro-UBM and UF-UBM particulate. Morphologically, the micro-UBM particulate appeared crystalline by scanning electron microscopy (SEM) imaging. The UF-UBM particulate had a more granular-like shape (Fig. 1A). The micro-UBM material had a relatively consistent size distribution, with most of the particulate ranging between 100 and 1000 μm (Fig. 1B). Most of the UF-UBM particulate ranged between 1 and 50 μm. We examined the biodegradability of the UBM scaffolds in an enzyme-rich controlled environment in vitro, to assess potential correlation between particulate size and expected resorption time in vivo. The micro-UBM showed a lower degradation rate compared to the UF-UBM as measured by loss of weight percentage loss (Fig. 1C).

We then investigated whether treatment with UBM could enhance wound repair and reduce scar formation in the cornea. First, we labeled the materials with Alexa Fluor 790 to track retention in the ocular space after injection into the subconjunctival space using near-infrared imaging. Athymic (nude) mice were used for these studies so the dye could be imaged without an autofluorescent background from the fur. Consistent with the in vitro degradation assay, micro-UBM displayed longer retention in the subconjunctival space compared to UF-UBM as measured by near-infrared imaging (Fig. 1D). In addition, we found that the scaffolds remained highly localized in the injection site and did not diffuse.

To evaluate the impact on wound healing in the cornea, micro-UBM and UF-UBM were applied to a corneal debridement wound model in mice. In this wound model, a 1.5-mm-diameter region in the central cornea is scraped to remove the epithelium leading to scar formation. The region of scar formation after injury was identified by photography (Fig. 1E, red dashed line). After blinded quantification of the corneas, we observed that UBM treatments (both micro-UBM and UF-UBM) significantly reduced the haze formation compared to a phosphate-buffered saline (PBS) control ($P < 0.0001$) (Fig. 1, E and F), suggesting a reduction in scar formation.

UBM injection inhibits myofibroblast differentiation

To further characterize the haze and scar formation after corneal injury, we evaluated vascularization and fibroblast development. Immunofluorescent staining of the injured cornea for CD31 revealed the vasculature in the limbus area after injury and treatment. In comparison with the relatively dim staining of CD31 in no injury controls, PBS-treated corneas demonstrated an increase of vasculature in the limbus area at 1 and 2 weeks after surgery, consistent with chronic inflammation and possible neovascularization. Micro-UBM–treated corneas showed some increase of vasculature in the limbus area at 1 week after surgery, but by week 2, the extent of vascularization decreased. The vasculature in the UF-UBM group remained low at both 1 and 2 weeks after injury (Fig. 2A). We next stained α-smooth muscle actin (αSMA) to assess the myofibroblast activation in the corneal stroma. During wound healing, the αSMA-expressing myofibroblasts are the key contributors to pathological scar formation (*29*, *30*). At 2 weeks after surgery, PBS-treated corneas showed a higher level of αSMA^+ staining (indicated by white arrows), suggesting an increase in myofibroblasts as compared to micro- and UF-UBM treatments (Fig. 2B).

To further investigate the myofibroblasts, we used flow cytometry to characterize different fibroblast subsets. We applied a gating scheme to identify three primary corneal stromal cell lineages using the markers $CD29^+\alpha SMA^+$, $CD29^+S100^+$, and $CD29^+SCA1^+$ (fig. S1). CD29 (β-integrin) is a broad marker for multiple cell types that is highly expressed in stromal cells. Because of the lack of precision around fibroblast-specific markers, we used CD29 (as positive marker) in combination with CD45, CD31, CD11b, and CD34 as exclusion markers. Different subsets of fibroblast may drive different pathological consequences, some of which are immune dependent. For example, αSMA is a classic marker for myofibroblasts, which function in fibrosis, and has been associated with excessive deposition of haze and scar formation (*31*). S100 is linked with angiogenesis and tumorigenesis (*32*, *33*), whereas Sca-1 (Ly6a) is associated with immature or progenitor mesenchymal stromal cells (*34*).

At 2 weeks after injury, we found a greater density (more than 50%) of corneal stromal cells ($CD45^-CD31^-CD34^-CD29^+$) in the wounded cornea without treatment (fig. S1). UF-UBM treatment significantly reduced the $CD29^+S100^+$ cell population ($P < 0.01$), and $CD29^+\alpha SMA^+$ cells significantly decreased with both micro- and UF-UBM treatments (PBS versus micro-UBM $P < 0.05$, PBS versus UF-UBM $P < 0.01$). $CD29^+Sca1^+$ fibroblasts did not change with UBM treatment (Fig. 2C). To further investigate fibrotic changes of wounded corneas with different treatments, we performed NanoString analysis using the nCounter Fibrosis Panel. Consistent with our earlier findings with flow cytometry where fibroblast-associated cell surface markers decreased with treatment, the expression of fibrosis-associated genes also significantly decreased with UF-UBM treatment compared to

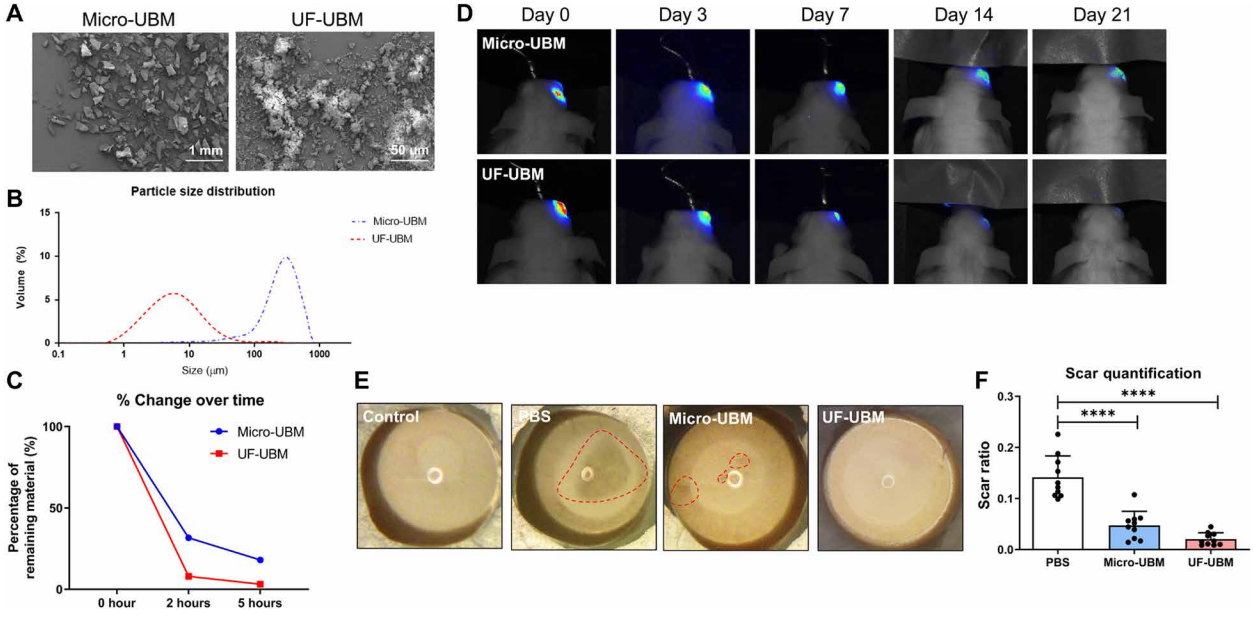

Fig. 1. UBM particulate reduced corneal scarring after debridement wound. (**A**) SEM images of micro- and UF-UBM. Scale bars, 1 mm (micro-UBM) and 50 μm (UF-UBM). (**B**) Particle size distribution curve of micro- and UF-UBM. The size distribution of micro-UBM is approximately 100 to 1000 μm, and the size distribution of UF-UBM is 1 to 50 μm. (**C**) Percentage of volume change over time of micro- and UF-UBM in vitro. The remaining weight percentage was 18 and 3% for micro- and UF-UBM after 5 hours, respectively. (**D**) Resorption of micro- and UF-UBM in vivo. By 21 days after surgery, the fluorescence of tagged UF-UBM diminished, while that of tagged micro-UBM remained in the ocular region. (**E**) Gross photos of wounded eye globes treated with PBS, micro-UBM, and UF-UBM at 14 days after surgery. (**F**) Quantification of corneal scar ratio of PBS-, micro-UBM–, and UF-UBM–treated corneas. ****$P < 0.0001$.

the PBS-treated control (Fig. 2, D and E). We performed a differential expression analysis of the NanoString data and found that UBM treatments down-regulated a large set of fibrosis-associated genes when normalized to PBS-treated control (Fig. 2, C and D). Markedly, UF-UBM treatment demonstrated statistical significance in down-regulated genes including *Col3a1*and *Acta2*, which are closely associated with scar-related extracellular deposition and myofibroblast activation (*35*) ($P < 0.05$). The stromal cells in both UBM treatment groups expressed lower levels of the fibroblast activation markers *Fap* and *Acta2*, as well as decreased expression of ECM proteins (*Col3a1*, *Eln*, and *Col14a1*) and angiogenesis markers (*Tek* and *Pdgfb*) (Fig. 2, C and D).

UBM treatment increases type 2 immune response

Biological scaffolds applied to the cornea wounds induced a type 2 immune response characterized by the presence of T_H2 cells, eosinophils, and alternatively activated (M2) macrophages (*23*, *36*). This type 2 immune polarization is perpetuated by IL-4 production, which initiates a program of tissue repair (*37*). Using flow cytometric analysis of cells isolated from the injured corneas, we found that IL-4 expression significantly increased in corneal T cells and eosinophils at 1 week after injury after both micro- and UF-UBM treatments (T cells: PBS versus micro-UBM $P < 0.01$, PBS versus UF-UBM $P < 0.05$; eosinophils: PBS versus micro-UBM $P < 0.001$, PBS versus UF-UBM $P < 0.05$) (Fig. 3, A and B). The response was more pronounced in micro-UBM compared to UF-UBM at the time point analyzed, which might be due to the degradation difference between the two materials. We did not observe any significant phenotypic changes in other immune cells in the wounded corneal environment (figs. S2 and S3).

We also evaluated the expression of cytokines in the draining lymph node (cervical) and found that IL-4–producing T cells (T_H2) significantly increased with micro- and UF-UBM treatments compared to PBS-treated controls at 1 week after injury, highlighting a cross-talk between local immune cells and those residing in peripheral lymphoid tissues (PBS versus micro-UBM $P < 0.01$, PBS versus UF-UBM $P < 0.05$) (Fig. 3, C and D). At 2 weeks after injury, the total number of IL-4–producing T cells in the cervical lymph node decreased compared to levels found at 1 week after injury. In the UF-UBM group, the IL-4–producing T cell numbers reduced to levels similar to the PBS group, while in micro-UBM–treated corneas, the IL-4–producing T cells remained elevated ($P < 0.001$). (Fig. 3, E and F). UBM treatments decreased interferon-γ–positive ($IFN\gamma^+$)–producing T cells (T_H1) compared to the PBS-treated control at 2 weeks after surgery (Fig. 3, D to F). UBM treatments did not show a significant impact on the number of $IL\text{-}17^+$–producing T cells (T_H17) in the draining lymph nodes.

Eosinophils play critical roles in UBM-suppressed corneal scarring

Given that eosinophils were a major source of IL-4 in the cornea with UBM treatment (Fig. 3), we sought to determine whether these cells played a role in corneal wound healing and biomaterial response. UBM treatments were applied to cornea wounds in $Gata1^{-/-}$ mice that lack eosinophils. The proregenerative effect of the UBM biomaterials was completely ablated in the $Gata1^{-/-}$ mice with identical scar formation and haze development regardless of UBM treatment (Fig. 4, A to C). Immunofluorescence analysis confirmed no reduction of vasculature in UMB-treated $Gata1^{-/-}$ mice, suggesting that UBM enhanced corneal repair in an eosinophil-dependent

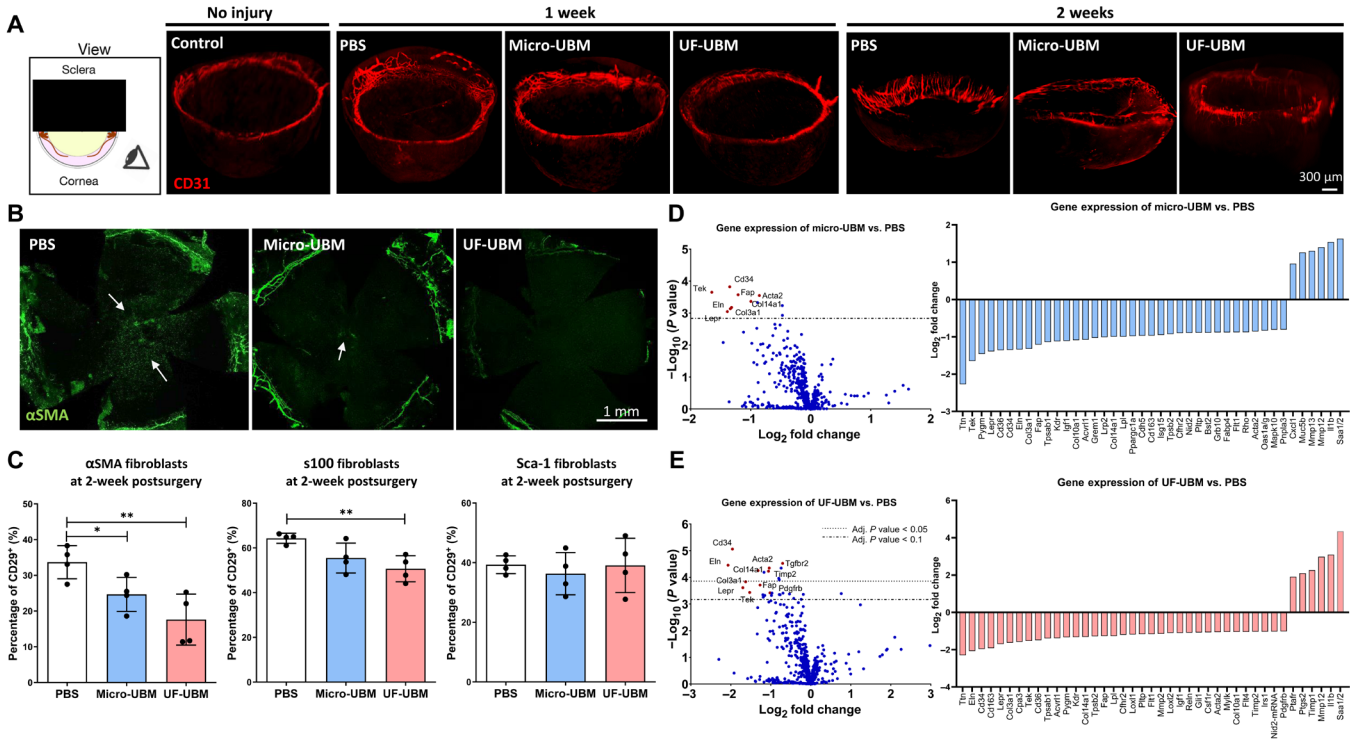

Fig. 2. Corneal stromal cell activation after corneal injury in vivo. (**A**) Three-dimensional light sheet microscopy imaging of CD31-stained PBS-, micro-UBM-, and UF-UBM–treated corneas. Scale bar, 300 μm. (**B**) Whole corneal immunostaining of α-SMA in PBS-, micro-UBM–, and UF-UBM–treated corneas. Scale bar, 1 mm. (**C**) Multiparametric flow cytometry analysis of α-SMA$^+$, s100$^+$, and Sca-1$^+$ corneal fibroblasts (CD45-CD34-CD31-CD29$^+$). $n = 4$, $^*P < 0.05$ and $^{**}P < 0.01$. (**D**) Volcano plot of micro-UBM–treated corneas normalized to PBS-treated corneas; the dotted line denotes $P = 0.1$. Right: Differential expression of the top 50 fibrosis-related genes in the micro-UBM group compared to PBS, 2 weeks after surgery ($n = 3$). (**E**) Volcano plot of UF-UBM–treated corneas normalized to PBS treated corneas; the top dotted line denotes $P = 0.05$, and the bottom dotted line denotes $P = 0.1$. Right: Differential expression of the top 50 fibrosis-related genes in the UF-UBM group compared to PBS, 2 weeks after surgery ($n = 3$).

manner (Fig. 4B). Furthermore, there was no increase in IL-4$^+$–producing T cells in the draining lymph nodes in Gata1$^{-/-}$ mice, suggesting the importance of cross-talk between eosinophils residing in the local tissue and T cells in the peripheral secondary lymphoid organs (Fig. 4D). We further characterized UBM-associated myofibroblasts in eosinophil-depleted mice using flow cytometry. There was no reduction in CD29$^+$αSMA$^+$ fibroblast activation in Gata1$^{-/-}$ mice regardless of UBM treatments (Fig. 4E). Together, these observations supported the notion that UBM promotes an eosinophil-mediated type 2 immune response, which subsequently enhances corneal wound healing.

DISCUSSION

The concept of immune privilege in the eye refers to minimal immune infiltration and inflammatory responses to preserve vision and maintain ocular architecture (*38*). This immune privilege protects the eye from swelling or other tissue changes caused by minor inflammatory response, so visual function is maintained. However, there is the Yin and Yang of immune privilege in the eye (*39*). The lack of blood vasculature and lymphatics limits the local immune cell populations; the absence of major histocompatibility complex class II$^+$ antigen–presenting cells negates CD4 T cells (*40*); and the local production of immunosuppressive factors such as TGF-β suppresses the inflammatory responses further (*41*). In the context of infection or injury, proregenerative immune cells such as alternatively activated macrophages and T_H2 cells are critical to tissue regeneration (*23*, *41*). Lacking natural activation of these cells in the eye, injuries to the cornea without intervention may lead to scar formation that impairs vision (*39*, *42*).

Biological therapies have been developed to modulate corneal immune response and improve corneal regeneration after injury, including stem cell and ECM therapies (*13*, *28*). ECM components from decellularized tissues can influence the immune response locally and systemically to facilitate wound healing processes such as angiogenesis, stem cell proliferation, and stimulating anti-inflammatory responses (*43*, *44*). UBM particulate in the present study has a highly complex compositional profile according to a previous proteomic analysis (*36*). Most ECM components such as collagen I, III, IV, VII, and laminin survived after decellularization processes. Non-ECM residuals in the UBM can act as damage-associated molecular patterns (DAMPs) to modulate immune response and promote wound healing (*45*). Direct implantation of UBM materials drives type 2 immune response by actively recruiting alternatively activated macrophages, IL-4–producing CD4$^+$ T cells, and eosinophils (*24*), creating a proregenerative microenvironment for tissue regeneration in, for example, muscle tissue (*36*). The natural degradation of UBM also releases bioactive components, including ligands, cryptic peptides, and matrix-bound nanovesicles (MBVs) (*46*, *47*). These components are slowly released to the environment during degradation, actively presenting biological cues such as small RNAs and miRNAs that can have a prolonged proregenerative impact on the host (*46*).

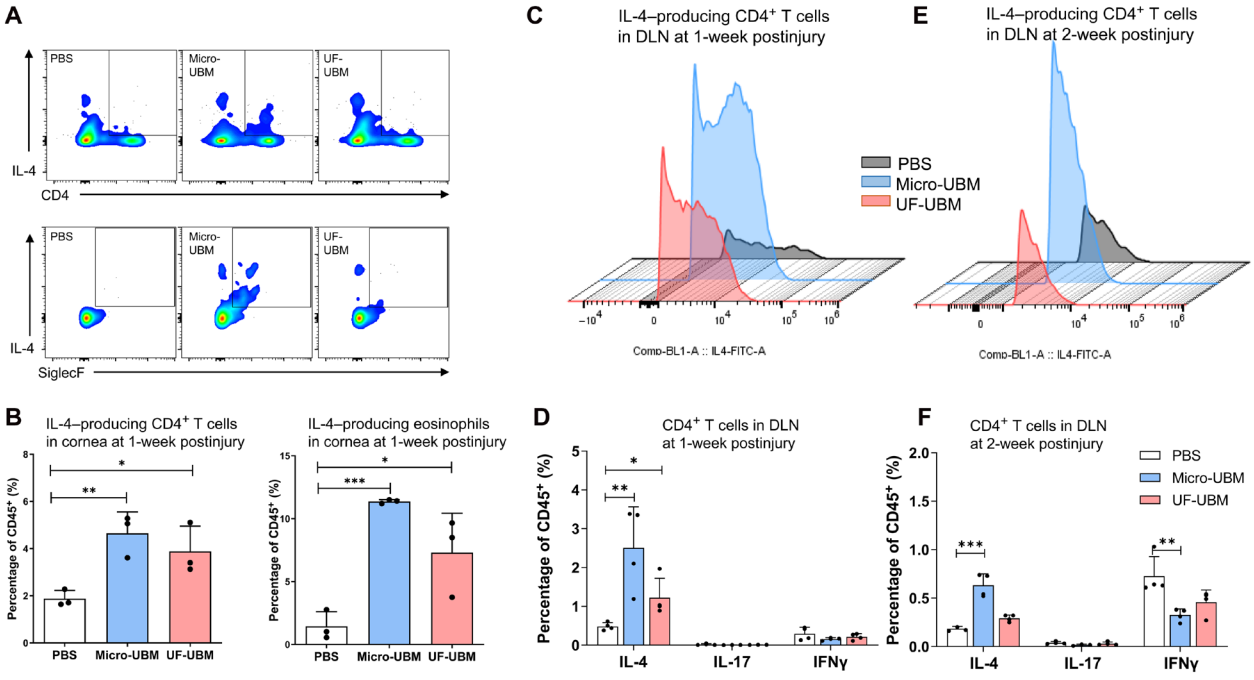

Fig. 3. Immune response in wounded corneas and draining lymph nodes (DLN). (**A**) Multiparametric flow cytometry analysis of IL4$^+$ CD4$^+$ T cells (CD45$^+$CD3$^+$) and IL-4$^+$ SiglecF$^+$ myeloid cells (CD45$^+$CD11b$^+$) isolated from the wounded cornea 1 week after surgery. (**B**) IL-4 expression in CD4$^+$ T cells and SiglecF$^+$ eosinophils at 1 week after surgery ($n = 3$, each data point represents cells collected from five corneas). *$P < 0.05$, **$P < 0.01$, and ***$P < 0.001$. (**C**) IL-4 expression in CD4$^+$ T cells isolated from draining lymph nodes at 1 week after surgery. (**D**) IL-4, IL-17, and IFNγ expression in CD4$^+$ T cells at 1 week after surgery. (**E**) IL-4 expression in CD4$^+$ T cells isolated from draining lymph nodes at 2 weeks after surgery. (**F**) IL-4, IL-17, and IFNγ expression in CD4$^+$ T cells at 2 weeks after surgery. $n = 4$, *$P < 0.05$, **$P < 0.01$, and ***$P < 0.001$.

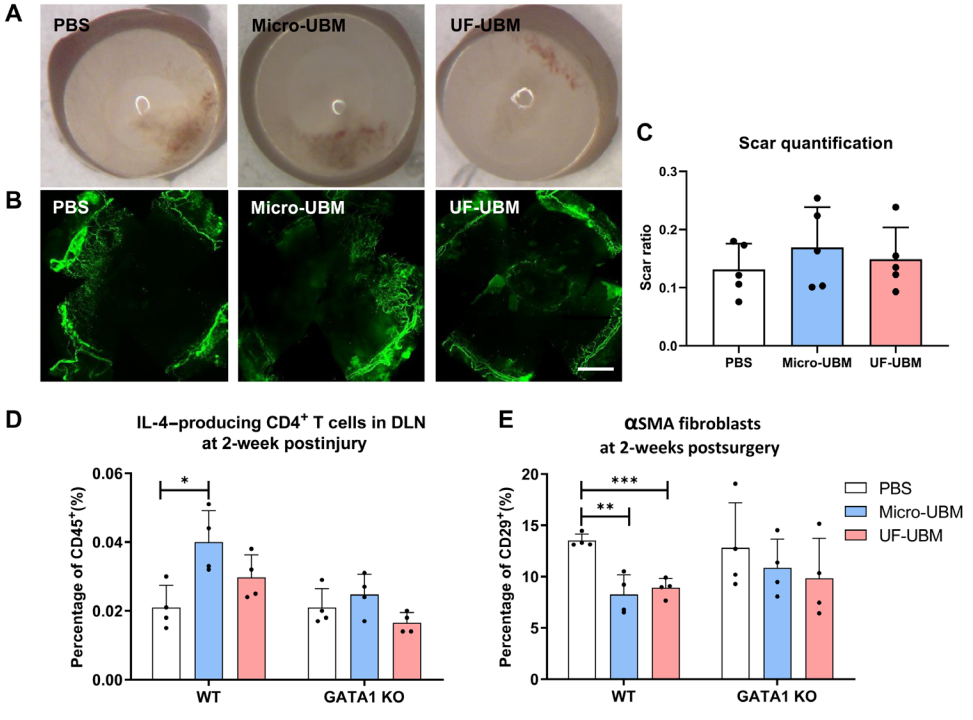

Fig. 4. Corneal scarring in Gata1$^{-/-}$ mice. (**A**) Gross photos of wounded corneas of Gata1$^{-/-}$ mice treated with PBS, micro-UBM, and UF-UBM. (**B**) Immunostaining of α-SMA in PBS-, micro-UBM–, and UF-UBM–treated Gata1$^{-/-}$ corneas. Scale bar, 1 mm. (**C**) Scar quantification of Gata1$^{-/-}$ mice at 2 weeks after surgery. $n = 4$. (**D**) IL-4 expression in CD4$^+$ T cells isolated from draining lymph nodes of wild-type (WT) and Gata1$^{-/-}$ mice at 2 weeks after surgery. $n = 4$, *$P < 0.05$. (**E**) α-SMA$^+$ corneal fibroblast population isolated from wounded corneas of WT and Gata1$^{-/-}$ mice at 2 weeks after surgery. $n = 4$, **$P < 0.01$ and ***$P < 0.001$.

Cryptic peptides promote in vivo recruitment of progenitor cells in a murine digit amputation model (*48*). MBVs protect retinal ganglion cell death and axon degeneration against ischemia-induced injury and down-regulate proinflammatory gene expressions including IL-1β, TNF-α, and IL-6 (*49*). In our study, we directly injected UBM particulate of micro- and UF-scales into the subconjunctival space. Proteinase in the tear film likely gradually degraded the UBM particulate, releasing bioactive factors that contributed to modulation of the immune response.

Particle size has been extensively studied in the context of biomaterials development for drug delivery (*50*, *51*). One of the advantages of UF-UBM particulate over micro-UBM particulate in the cornea application is their small size which allows them to be easily applied to the eye without altering vision while still remaining immunologically active. The smaller size allows more diffusion and relatively faster degradation and is potentially more desirable for immune recognition. As compared to micro-UBM, UF-UBM suspension presents an effective mode of drug administration and a reasonable residence time (about 7 days) on the ocular surface after subconjunctival injection, suggesting UF-UBM potential for ophthalmic applications. We found that injection with UBM induced a potent type 2 immune response consisting of IL-4–producing eosinophils in the local corneal tissue and T_H2 cells in the peripheral draining lymph node. This up-regulation of type 2 immune response remained for more than 14 days in the micro-UBM group, while in the UF-UBM group, this up-regulation peaked at day 7 then decreased to pretreatment levels. Ablation of eosinophils using $Gata1^{-/-}$ mice diminished the prohealing outcome regardless of UBM treatment, suggesting that eosinophils were required for UBM-facilitated corneal wound healing.

During the tissue repair process, stromal cells proliferate and synthesize new ECM to repair and replace damaged tissue (*52*). If these cells are not regulated, they develop into a pathological positive feedback loop where more and more ECM is deposited. Especially in the cornea, excessive deposition of ECM can cause severe haze and vision impairment (*53*). Our results suggest that myofibroblast differentiation in the cornea after injury was orchestrated by these immunological shifts induced by the UBM microenvironment. Early studies of stromal cell activation often rely on cell morphology, and it is challenging to define stromal cell phenotypes due to a lack of definitive markers (*54*, *55*). We subset stromal cells into three distinct populations: $CD29^+\alpha SMA^+$, $CD29^+S100^+$, and $CD29^+SCA1^+$. We found that UBM inhibited $CD29^+\alpha SMA^+$ myofibroblasts and $CD29^+S100^+$ fibroblasts, whereas $CD29^+SCA1^+$ populations remained mostly unchanged. Evaluating gene expression using the NanoString fibrosis panel enabled us to gain a physiological understanding of corneal cell, including stromal and epithelial cell expression patterns after injury. Significantly reduced expression of fibrosis genes, such as *Acta2*, *Col3a1*, and *Eln*, suggests a less activated myofibroblastic phenotype of corneal stromal cells in the UF-UBM–treated group.

A major endeavor in the field of regenerative immunology has been to understand how different immune cells respond and communicate locally and systemically after biomaterial implantation. Our data demonstrated an immune cross-talk between eosinophils in the local tissue and T cells in the peripheral lymphoid organ. Eosinophils can be seen at the corneal periphery near the limbus area (*56*). Eosinophils are equipped with various tissue damage sensing mechanisms, including DAMPs, which allow them to release tissue-repairing molecules and stimulate the adaptive immune responses (*57*). Previous studies found eosinophil depletion–impaired muscle and liver repair in a murine model (*58*, *59*), revealing the potentially critical role of IL-4–secreting eosinophils in tissue repair and regeneration. IL-4 is a multifunctional, pleiotropic cytokine that is the signature of T_H2 response. Emerging evidence suggests that IL-4 and T_H2 responses are essential for tissue regeneration (*60*). Although T_H2 response and eosinophils have been extensively reported in ophthalmology, they are often associated with an allergic response, keratitis, or dry eye (*61*, *62*). To our knowledge, the proregenerative role of eosinophils or type 2 immune response has not been reported in ocular repair and regeneration. In this study, we showed that eosinophil's involvement in the cornea was necessary for orchestrating the adaptive immunity in UBM microenvironment and polarization of T_H2 cells. Detailed analysis of immune cells showed that IL-4 was highly up-regulated in the cornea and draining lymph nodes in wild-type (WT) mice treated with UBM. However, ablation of eosinophils prevented the differentiation of T_H2 cells, suggesting that they play a critical role in the initiation of this process. The connection between eosinophils and adaptive immunity in the cornea is unknown. There is evidence that eosinophils and dendritic cells act in concert to activate and polarize T cells in the draining lymph node (*63*). Another possible explanation is that eosinophils in the cornea produce the T cell–polarizing cytokine IL-4, which is drained to the peripheral lymph node and directly induces the differentiation of T_H2 effector cells (*64*, *65*). Further research is needed to understand how T_H2 proregenerative and allergic responses differ. Moreover, the diversity of patient health and immune status may affect therapeutic response. For example, in cases where a patient's immune system is compromised, such as in advanced age, underlying metabolic disorder, or immunosuppressant drug therapies, the composition and quality of the therapeutic immune response will be altered. As a result, the response to UBM treatment in these patient populations may be diminished. Further research into how the underlying immune status of patients affects response to regenerative immunotherapies will be critical to understand as these technologies reach more widespread clinical use.

MATERIALS AND METHODS

Characterization of UBM materials

The micro-UBM and UF-UBM were provided by ACell Inc. UBM is derived from decellularized basal and tunica propria layers of porcine urinary bladder tissue and includes a complex mixture of intracellular and extracellular proteins (*36*). Lamina propria and epithelial basement membrane layers were isolated from porcine bladder and processed according to proprietary internal ACell Inc. procedures. The UBM was then lyophilized and milled processed into micro-UBM or UF-UBM particulate that are amenable to delivery into the cornea by injection into the conjunctival space. The UBM materials were terminally sterilized using electron beam irradiation method.

Scanning electron microscopy

A thin layer of UBM particulate was mounted on adhesive metallic tape and sputter coated with 3.5 nm of gold. The samples were viewed with a JEOL JCM-6000 (JEOL Ltd.) SEM at magnifications ranging from 20× to 500×.

Particle size analysis

The relative particle size distribution was measured for each sample over the particle size range of 0.1 and 1000 μm (Mastersizer, Malvern Instruments Ltd.).

Material degradation

An in vitro single enzyme (Proteinase K) test model was developed to investigate potential differences in relative degradation rates between experimental groups. Approximately 20 mg of micro-UBM and UF-UBM was weighed and then transferred to 2-ml protein LoBind tubes. A working concentration of Proteinase-K (0.415 mg/ml) (Sigma-Aldrich) enzyme in 1× PBS was used for sample degradation. Samples were incubated in a dry oven at 37°C for 2 and 5 hours. At the designated time point, samples were centrifuged at 4°C at 1500 x*g* for 5 min. All fluids were extracted from the samples and discarded. The degraded sample fibers found at the bottom of the tube (pellet) were washed with 1 ml of water and centrifuged again at 1500 x*g* for 5 min to remove additional salts. The remaining fluid was then discarded, and samples were dried overnight for weight measurement using analytical balance.

Murine corneal debridement wound model and treatment

All surgical procedures were performed under the guidelines of the Johns Hopkins University Animal Care and Use Committee, protocol number: MO17M308. Male adult BALB/C mice (8 to 12 weeks old), Gata1 knockout (Gata1$^{-/-}$) mice, and IL4-IRES-eGFP (4get) mice were purchased from the Jackson laboratory (ME, USA). All experimental groups had a sample size of $n \geq 3$.

The murine corneal wound model was adapted from a previous study (*66*). Mice were weighted and anesthetized with ketamine HCl (90 mg/kg) (Vetone, ID, USA) and xylazine HCl (10 mg/kg) (Vetone) injection. Proparacaine hydrochloride ophthalmic eye drops (Sandoz, Holzkirchen, Germany) were applied after the mice were sedated. The center area of the cornea was marked by a 1.5-mm biopsy punch, and the epithelium layer was removed within the area by a 1.5-mm flat blade (Fine Science Tools, CA, USA). After epithelium removal, extra force was used on the wounded area using the same flat blade to disrupt the basement membrane, and a volume of 50-μl PBS solution with either no UBM addition or with micro-UBM or UF-UBM (10 mg/ml) (Acell, MD, USA) suspended was injected to the subconjunctival space of the wounded eye. After injection, drops of PBS solution were applied to both wounded and unwounded eyes to keep the eyes moist until the mice recovered from anesthesia.

UBM resorption in vivo

We tagged the micro-UBM and UF-UBM with Alexa Fluor 790 NHS Ester (Thermo Fisher Scientific, MA, USA). Briefly, UBM (10 mg/ml) was suspended in PBS and sonicated for 60 min. One hundred–microgram dye was dissolved in 40 μl of dimethyl sulfoxide and then added to each UBM suspension. The suspensions were gently shaken at room temperature for 1 hour and washed three times with PBS. After washing in PBS for another 18 hours at 4°C, the UBM was collected and resuspended in PBS, followed by injection into male adult nude mice (8 weeks old from the Jackson laboratory) subconjunctival space. The labeled UBM was imaged with LI-COR near-infrared scanner on days 0, 3, 7, 14, and 21 after injection.

Scar formation and quantification

At 14 days after surgery, the mice were euthanized, and the eye globes were collected. The picture of each globe was taken under a surgical microscope (Nikon, Japan), and the scar areas and cornea areas were determined with ImageJ. The ratio was quantified as: scar ratio = A_s (scar area)/A_c (whole corneal area).

Flow cytometry

Immune profile in wounded corneas

Wounded corneas were collected from each experimental group (PBS, micro-UBM, and UF-UBM); five corneas were pooled for one "flow cytometry sample." Corneas in each group were digested in RPMI 1640 media containing Liberase^{TM} TL (Thermolysin Low) (0.5 mg/ml) (Sigma-Aldrich, MO, USA) and deoxyribonuclease I (0.2 mg/ml) (Roche, Basel, Switzerland) for 45 min. Digested tissues were grinded through a 70-μm filter. Cell suspensions were centrifuged and washed, and each cell pellet was resuspended in 200 μl of PBS for staining. The antibodies used are listed in Table 1.

Immune profile in draining lymph nodes

Draining lymph nodes (submandibular lymph nodes) were collected and ground through a 70-μm filter. Cells were collected after centrifugation and washing with PBS. Lymphocytes were stimulated for 4 hours with cell stimulation cocktail (plus protein transport inhibitors) (eBioscience, CA, USA), followed by staining of surface markers. After permeabilization and fixation of cells, cytokines IL-17 and IFNγ were stained for 4get mice, and IL-17, IL-4, and IFNγ were stained for WT and Gata1$^{-/-}$ mice. The antibodies used were listed in Table 2.

Fibroblast subsets in wounded corneas

Corneas were collected and digested following the methods listed in "Immune profile in wounded corneas". For fibroblast staining, two corneas were pooled as one flow cytometry sample. The antibodies used for fibroblast panel were listed in Table 3.

Immunostaining

Dissected corneas were fixed in 100% methanol at −20°C for 30 min and permeabilized with PBS containing 0.25% Triton X-100 (PBST). The cornea samples were blocked with 1% goat serum and 1% bovine serum albumin (BSA) in PBST for 30 min and stained with rabbit anti-mouse αSMA (Abcam, Cambridge, United Kingdom) overnight at 4°C. Following washing with PBST, corneas were stained with goat anti-rabbit 633 (Abcam) for 2 hours at room temperature and mounted flat in SlowFade Diamond Antifade Mountant (Thermo Fisher Scientific). Zeiss Apotome microscope was used for fluorescence imaging.

Light sheet fluorescence imaging

Mouse eyes were harvested at 1 and 2 weeks after operation and immediately fixed in 4% paraformaldehyde at 4°C for 16 to 24 hours.

Table 1. List of antibodies used for wounded cornea flow cytometry.

Antibodies	Fluorescence	Concentration
CD45	BV605	1:100
CD11b	AF700	1:250
CD11c	Percp-Cy5.5	1:250
F480	PE-Cy7	1:150
Ly6g	Pacific Blue	1:250
Ly6c	BV510	1:250
SiglecF	PE-594	1:200
CD3	PE	1:150
CD4	APC	1:250
CD8	BV711	1:200
Live-dead	eFluor 780 viability	1:1000

Table 2. List of antibodies used for draining lymph node flow cytometry.

Antibodies	Fluorescence	Concentration
CD45	V500	1:100
CD3	PE (4get) AF488 (WT and Gata1$^{-/-}$)	1:150
CD4	PE-Cy7	1:250
NK 1.1	BV605	1:200
γδ-TCR	PE-594	1:200
CD90.2	Pacific Blue	1:250
CD19	Percp Cy-5.5	1:250
IL17	AF700	1:250
INF-γ	APC	1:150
IL4	GFP (4get) PE (WT and Gata1$^{-/-}$)	– 1:200
Live-dead	eFluor 780 viability	1:1000

Table 3. List of antibodies used for corneal fibroblast flow cytometry.

Antibodies	Fluorescence	Concentration
CD45	BV605	1:150
CD31	BV421	1:100
CD34	PerCP-Cy5.5	1:100
CD3	AF488	1:200
CD29	APC-Cy7	1:100
CD90.2	AF700	1:100
CD140a	PE-Cy7	1:100
Sca-1	PE-Dazzle 594	1:200
S100	PE	1:100
α-SMA	APC	1:100
Live-dead	Viability Aqua	1:1000

Eyes were then cleared using the clear, unobstructed brain/body imaging cocktails and computational analysis (CUBIC) protocol (*67*). Samples were incubated at 37°C for 16 to 24 hours in a 12-ml solution of CUBIC1 [25% (w/w) urea (Sigma-Aldrich, U5128), 25% (w/w) Quadrol (Sigma-Aldrich), 15% (w/w) Triton X-100 (Sigma-Aldrich) in dH_2O], diluted 50% (v/v) in dH_2O, and then incubated at 37°C in 100% CUBIC1 for 2.5 days, replacing with fresh solution twice per day. Samples were subsequently washed three times in 0.1% Triton X-100 in PBS, blocked for 16 to 24 hours in 10% BSA and 0.1% Triton X-100 in PBS, and then stained with mouse/rat CD31/platelet endothelial cell adhesion molecule–1 antibody (R&D Systems / Bio-Techne, AF3628) 1:100 in blocking buffer for 24 to 36 hours. After a 6- to 8-hour wash with 0.1% Triton X-100, samples were stained with donkey anti-goat Alexa Fluor 568 secondary antibody (Invitrogen, CA, USA) 1:100 in blocking buffer for 24 hours, protected from light, and then washed for 14 to 18 hours in 0.1% Triton X-100 in PBS. All washing, blocking, and staining occurred at room temperature with gentle agitation. Last, samples were incubated for 6 to 8 hours at 37°C in 12 ml of CUBIC2 [25% urea (w/w), 50% sucrose (w/w), and 10% (w/w) triethanolamine made fresh in dH_2O] solution diluted 50% (v/v) in dH_2O and then incubated for 24 hours at 37°C in 100% CUBIC2. The cleared, stained mouse eyes were whole-mounted and visualized using a LaVision BioTec UltraMicroscope II light sheet fluorescent microscope equipped with a LVMI-Fluor objective at 1× optical zoom. Imaging occurred immediately after mounting in immersion medium (Sigma-Aldrich) with a sheet thickness of 5 μm (numerical aperture = 0.154), an axial step size of 2.5 μm, an excitation at 561 nm, and a 590/33 nm emission filter. The resulting three-dimensional volumes were reconstructed using Imaris software (Oxford Instruments).

NanoString

At day 14 (2 weeks after injury), wounded corneas were harvested and homogenized in TRIzol reagent by an automated tissue homogenizer (Bead Ruptor 12, Omni International). All mRNA was isolated and purified using the RNeasy PLUS microkit system (Qiagen, Hilden, Germany) for NanoString analyses. Samples harvested on day 14 were evaluated by the NanoString Fibrosis panel (XT-CSO-MFIB2-12, NanoString Technologies Inc.). One hundred nanograms of mRNA from each sample was added to a barcoded probe-set mixture and hybridized for 20 hours at 65°C. Hybridized samples were further processed using the NanoString Prep Station operating under high sensitivity mode, and mRNA target transcripts were counted using the nCounter digital analyzer system (NanoString).

Statistical analysis

The flow cytometry samples were tested using Attune NxT Flow cytometer (Thermo Fisher Scientific). The flow cytometry data were computed using FlowJo v10 software and were displayed as the means ± SD. Multiple *t* test was performed using GraphPad Prism v8, with $P < 0.05$ considered statistically significant. NanoString data were analyzed using nSolver software (v3.0, NanoString). The top 50 differentially regulated genes were uploaded into the DAVID functional annotation tool, and Gene Ontology was run to calculate significantly enriched gene sets.

SUPPLEMENTARY MATERIALS

Supplementary material for this article is available at http://advances.sciencemag.org/cgi/content/full/7/16/eabe2635/DC1

View/request a protocol for this paper from *Bio-protocol*.

REFERENCES AND NOTES

1. S. A. Schendel, *The Orbit, An Issue of Oral and Maxillofacial Surgery Clinics-E-Book* (Elsevier Health Sciences, 2012), vol. 24.
2. W. J. Dupps Jr., S. E. Wilson, Biomechanics and wound healing in the cornea. *Exp. Eye Res.* **83**, 709–720 (2006).
3. S. E. Wilson, R. R. Mohan, R. R. Mohan, R. Ambrósio Jr., J. Hong, J. Lee, The corneal wound healing response: Cytokine-mediated interaction of the epithelium, stroma, and inflammatory cells. *Prog. Retin. Eye Res.* **20**, 625–637 (2001).
4. M. A. Stepp, G. Tadvalkar, R. Hakh, S. Pal-Ghosh, Corneal epithelial cells function as surrogate Schwann cells for their sensory nerves. *Glia* **65**, 851–863 (2017).
5. S. E. Wilson, Corneal myofibroblast biology and pathobiology: Generation, persistence, and transparency. *Exp. Eye Res.* **99**, 78–88 (2012).
6. M. Rocher, P.-Y. Robert, A. Desmoulière, The myofibroblast, biological activities and roles in eye repair and fibrosis. A focus on healing mechanisms in avascular cornea. *Eye* **34**, 232–240 (2020).
7. A. S. Menko, J. L. Walker, M. A. Stepp, Fibrosis: Shared lessons from the lens and cornea. *Anat Rec (Hoboken)* **303**, 1689–1702 (2020).

8. J. L. Funderburgh, M. L. Funderburgh, M. M. Mann, L. Corpuz, M. R. Roth, Proteoglycan expression during transforming growth factor β-induced keratocyte-myofibroblast transdifferentiation. *J. Biol. Chem.* **276**, 44173–44178 (2001).
9. S. Shukla, S. S. Shanbhag, F. Tavakkoli, S. Varma, V. Singh, S. Basu, Limbal epithelial and mesenchymal stem cell therapy for corneal regeneration. *Curr. Eye Res.* **45**, 265–277 (2020).
10. T. A. Blenkinsop, B. Corneo, S. Temple, J. H. Stern, Ophthalmologic stem cell transplantation therapies. *Regen. Med.* **7**, 32–39 (2012).
11. R. Mohan, A. R. Muralidharan, Steroid induced glaucoma and cataract. *Indian J. Ophthalmol.* **37**, 13–26 (1989).
12. W.-N. Ku, C.-J. Lin, Y.-Y. Tsai, The rescue effect of adalimumab in the treatment of refractory pediatric panuveitis complicated with steroid-induced glaucoma. *Taiwan J. Ophthalmol.* **8**, 164–167 (2018).
13. S. Basu, A. J. Hertsenberg, M. L. Funderburgh, M. K. Burrow, M. M. Mann, Y. Du, K. L. Lathrop, F. N. Syed-Picard, S. M. Adams, D. E. Birk, J. L. Funderburgh, Human limbal biopsy–derived stromal stem cells prevent corneal scarring. *Sci. Transl. Med.* **6**, 266ra172 (2014).
14. J. Wu, Y. Du, M. M. Mann, J. L. Funderburgh, W. R. Wagner, Corneal stromal stem cells versus corneal fibroblasts in generating structurally appropriate corneal stromal tissue. *Exp. Eye Res.* **120**, 71–81 (2014).
15. P. Prabhasawat, P. Ekpo, M. Uiprasertkul, S. Chotikavanich, N. Tesavibul, Efficacy of cultivated corneal epithelial stem cells for ocular surface reconstruction. *Clin. Ophthalmol.* **6**, 1483–1492 (2012).
16. G. Totonelli, P. Maghsoudlou, M. Garriboli, J. Riegler, G. Orlando, A. J. Burns, N. J. Sebire, V. V. Smith, J. M. Fishman, M. Ghionzoli, M. Turmaine, M. A. Birchall, A. Atala, S. Soker, M. F. Lythgoe, A. Seifalian, A. Pierro, S. Eaton, P. de Coppi, A rat decellularized small bowel scaffold that preserves villus-crypt architecture for intestinal regeneration. *Biomaterials* **33**, 3401–3410 (2012).
17. F. G. Thankam, I. Chandra, C. Diaz, M. F. Dilisio, J. Fleegel, R. M. Gross, D. K. Agrawal, Matrix regeneration proteins in the hypoxia-triggered exosomes of shoulder tenocytes and adipose-derived mesenchymal stem cells. *Mol. Cell. Biochem.* **465**, 75–87 (2020).
18. A. T. Rowley, R. R. Nagalla, S. W. Wang, W. F. Liu, Extracellular Matrix-Based Strategies for Immunomodulatory Biomaterials Engineering. *Adv. Healthc. Mater.* **8**, 1801578 (2019).
19. J. L. Dziki, S. F. Badylak, Immunomodulatory biomaterials. *Curr. Opin. Biomed. Eng.* **6**, 51–57 (2018).
20. A. Vishwakarma, N. S. Bhise, M. B. Evangelista, J. Rouwkema, M. R. Dokmeci, A. M. Ghaemmaghami, N. E. Vrana, A. Khademhosseini, Engineering immunomodulatory biomaterials to tune the inflammatory response. *Trends Biotechnol.* **34**, 470–482 (2016).
21. B. N. Brown, J. E. Valentin, A. M. Stewart-Akers, G. P. McCabe, S. F. Badylak, Macrophage phenotype and remodeling outcomes in response to biologic scaffolds with and without a cellular component. *Biomaterials* **30**, 1482–1491 (2009).
22. B. M. Sicari, J. L. Dziki, B. F. Siu, C. J. Medberry, C. L. Dearth, S. F. Badylak, The promotion of a constructive macrophage phenotype by solubilized extracellular matrix. *Biomaterials* **35**, 8605–8612 (2014).
23. K. Sadtler, K. Estrellas, B. W. Allen, M. T. Wolf, H. Fan, A. J. Tam, C. H. Patel, B. S. Luber, H. Wang, K. R. Wagner, J. D. Powell, F. Housseau, D. M. Pardoll, J. H. Elisseeff, Developing a pro-regenerative biomaterial scaffold microenvironment requires T helper 2 cells. *Science* **352**, 366–370 (2016).
24. M. T. Wolf, S. Ganguly, T. L. Wang, C. W. Anderson, K. Sadtler, R. Narain, C. Cherry, A. J. Parrillo, B. V. Park, G. Wang, F. Pan, S. Sukumar, D. M. Pardoll, J. H. Elisseeff, A biologic scaffold–associated type 2 immune microenvironment inhibits tumor formation and synergizes with checkpoint immunotherapy. *Sci. Transl. Med.* **11**, eaat7973 (2019).
25. H. N. Jacobs, S. Rathod, M. T. Wolf, J. H. Elisseeff, Intra-articular injection of urinary bladder matrix reduces osteoarthritis development. *AAPS J.* **19**, 141–149 (2017).
26. B. J. Kwee, D. J. Mooney, Biomaterials for skeletal muscle tissue engineering. *Curr. Opin. Biotechnol.* **47**, 16–22 (2017).
27. A. J. Lechner, I. H. Driver, J. Lee, C. M. Conroy, A. Nagle, R. M. Locksley, J. R. Rock, Recruited monocytes and type 2 immunity promote lung regeneration following pneumonectomy. *Cell Stem Cell* **21**, 120–134.e7 (2017).
28. H. Yin, Q. Lu, X. Wang, S. Majumdar, A. S. Jun, W. J. Stark, M. P. Grant, J. H. Elisseeff, Tissue-derived microparticles reduce inflammation and fibrosis in cornea wounds. *Acta Biomater.* **85**, 192–202 (2019).
29. J. Baum, H. S. Duffy, Fibroblasts and myofibroblasts: What are we talking about? *J. Cardiovasc. Pharmacol.* **57**, 376–379 (2011).
30. B. Hinz, in *Wound Healing Biomaterials* (Elsevier, 2016), pp. 69–100.
31. K. E. Myrna, S. A. Pot, C. J. Murphy, Meet the corneal myofibroblast: The role of myofibroblast transformation in corneal wound healing and pathology. *Vet. Ophthalmol.* **12**, 25–27 (2009).
32. A. Robson, P. Allen, K. Hollowood, S100 expression in cutaneous scars: A potential diagnostic pitfall in the diagnosis of desmoplastic melanoma. *Histopathology* **38**, 135–140 (2001).
33. Q. Al-Ismaeel, C. P. Neal, H. Al-Mahmoodi, Z. Almutairi, I. Al-Shamarti, K. Straatman, N. Jaunbocus, A. Irvine, E. Issa, C. Moreman, A. R. Dennison, A. E. Sayan, J. M. Dearmid, P. Greaves, E. Tulchinsky, M. Kriajevska, ZEB1 and IL-6/11-STAT3 signalling cooperate to define invasive potential of pancreatic cancer cells via differential regulation of the expression of S100 proteins. *Br. J. Cancer* **121**, 65–75 (2019).
34. M. R. Namazi, M. K. Fallahzadeh, R. A. Schwartz, Strategies for prevention of scars: What can we learn from fetal skin? *Int. J. Dermatol.* **50**, 85–93 (2011).
35. L. Weng, M. L. Funderburgh, I. Khandaker, M. Geary, K. Davoli, J. Funderburgh, Transforming growth factor beta 3 of human corneal stromal stem cells plays a pivotal role in suppression of mouse corneal scar formation. *Invest. Ophthalmol. Vis. Sci.* **59**, –2289 (2018).
36. K. Sadtler, S. D. Sommerfeld, M. T. Wolf, X. Wang, S. Majumdar, L. Chung, D. S. Kelkar, A. Pandey, J. H. Elisseeff, Proteomic composition and immunomodulatory properties of urinary bladder matrix scaffolds in homeostasis and injury. *Semin. Immunol.* **29**, 14–23 (2017).
37. A. J. Allman, T. B. McPherson, S. F. Badylak, L. C. Merrill, B. Kallakury, C. Sheehan, R. H. Raeder, D. W. Metzger, Xenogeneic extracellular matrix grafts elicit a TH2-restricted immune response1. *Transplantation* **71**, 1631–1640 (2001).
38. J. W. Streilein, B. R. Ksander, A. W. Taylor, Immune deviation in relation to ocular immune privilege. *J. Immunol.* **158**, 3557–3560 (1997).
39. J. V. Forrester, H. Xu, Good news–bad news: The Yin and Yang of immune privilege in the eye. *Front. Immunol.* **3**, 338 (2012).
40. P. Hamrah, M. R. Dana, *Immune Response and the Eye* (Karger Publishers, 2007), vol. 92, pp. 58–70.
41. W. Yang, X. Zhao, Y. Tao, Y. Wu, F. He, L. Tang, Proteomic analysis reveals a protective role of specific macrophage subsets in liver repair. *Sci. Rep.* **9**, 2953 (2019).
42. M. M. Mobaraki, R. Abbasi, S. O. Vandchali, M. Ghaffari, F. Moztarzadeh, M. Mozafari, Corneal repair and regeneration: Current concepts and future directions. *Front. Bioeng. Biotechnol.* **7**, 135 (2019).
43. M. Scarritt, M. Murdock, S. F. Badylak, *Principles of Regenerative Medicine* (Elsevier, 2019), pp. 613–626.
44. M. C. Cramer, S. F. Badylak, Extracellular matrix-based biomaterials and their influence upon cell behavior. *Ann. Biomed. Eng.*, 2132–2153 (2020).
45. K. Daly, S. Liu, V. Agrawal, B. N. Brown, S. A. Johnson, C. J. Medberry, S. F. Badylak, Damage associated molecular patterns within xenogeneic biologic scaffolds and their effects on host remodeling. *Biomaterials* **33**, 91–101 (2012).
46. L. Huleihel, G. S. Hussey, J. D. Naranjo, L. Zhang, J. L. Dziki, N. J. Turner, D. B. Stolz, S. F. Badylak, Matrix-bound nanovesicles within ECM bioscaffolds. *Sci. Adv.* **2**, e1600502 (2016).
47. N. Mehrban, C. Pineda Molina, L. M. Quijano, J. Bowen, S. A. Johnson, J. Bartolacci, J. T. Chang, D. A. Scott, D. N. Woolfson, M. A. Birchall, S. F. Badylak, Host macrophage response to injectable hydrogels derived from ECM and α-helical peptides. *Acta Biomater.* **111**, 141–152 (2020).
48. V. Agrawal, S. Tottey, S. A. Johnson, J. M. Freund, B. F. Siu, S. F. Badylak, Recruitment of progenitor cells by an extracellular matrix cryptic peptide in a mouse model of digit amputation. *Tissue Eng. Part A* **17**, 2435–2443 (2011).
49. Y. van der Merwe, A. E. Faust, E. T. Sakalli, C. C. Westrick, G. Hussey, K. C. Chan, I. P. Conner, V. L. N. Fu, S. F. Badylak, M. B. Steketee, Matrix-bound nanovesicles prevent ischemia-induced retinal ganglion cell axon degeneration and death and preserve visual function. *Sci. Rep.* **9**, 3482 (2019).
50. O. Veiseh, J. C. Doloff, M. Ma, A. J. Vegas, H. H. Tam, A. R. Bader, J. Li, E. Langan, J. Wyckoff, W. S. Loo, S. Jhunjhunwala, A. Chiu, S. Siebert, K. Tang, J. Hollister-Lock, S. Aresta-Dasilva, M. Bochenek, J. Mendoza-Elias, Y. Wang, M. Qi, D. M. Lavin, M. Chen, N. Dholakia, R. Thakrar, I. Lacík, G. C. Weir, J. Oberholzer, D. L. Greiner, R. Langer, D. G. Anderson, Size- and shape-dependent foreign body immune response to materials implanted in rodents and non-human primates. *Nat. Mater.* **14**, 643–651 (2015).
51. J. I. Andorko, C. M. Jewell, Designing biomaterials with immunomodulatory properties for tissue engineering and regenerative medicine. *Bioeng. Trans. Med.* **2**, 139–155 (2017).
52. L. E. Tracy, R. A. Minasian, E. J. Caterson, Extracellular matrix and dermal fibroblast function in the healing wound. *Adv. Wound Care* **5**, 119–136 (2016).
53. J. L. Funderburgh, M. M. Mann, M. L. Funderburgh, Keratocyte phenotype mediates proteoglycan structure a role for fibroblasts in corneal fibrosis. *J. Biol. Chem.* **278**, 45629–45637 (2003).
54. M. D. Lynch, F. M. Watt, Fibroblast heterogeneity: Implications for human disease. *J. Clin. Invest.* **128**, 26–35 (2018).
55. J. M. Sorrell, A. I. Caplan, Fibroblast heterogeneity: More than skin deep. *J. Cell Sci.* **117**, 667–675 (2004).
56. A. Ozaki, W. Ishida, K. Fukata, A. Fukushima, H. Ueno, Phenotypic changes and inflammatory cell distribution in the cornea during development of experimental immune-mediated blepharoconjunctivitis. *Jpn. J. Ophthalmol.* **48**, 333–339 (2004).
57. T. Gong, L. Liu, W. Jiang, R. Zhou, DAMP-sensing receptors in sterile inflammation and inflammatory diseases. *Nat. Rev. Immunol.* **20**, 95–112 (2020).
58. J. E. Heredia, L. Mukundan, F. M. Chen, A. A. Mueller, R. C. Deo, R. M. Locksley, T. A. Rando, A. Chawla, Type 2 innate signals stimulate fibro/adipogenic progenitors to facilitate muscle regeneration. *Cell* **153**, 376–388 (2013).

59. Y. P. S. Goh, N. C. Henderson, J. E. Heredia, A. R. Eagle, J. I. Odegaard, N. Lehwald, K. D. Nguyen, D. Sheppard, L. Mukundan, R. M. Locksley, A. Chawla, Eosinophils secrete IL-4 to facilitate liver regeneration. *Proc. Natl. Acad. Sci. U.S.A.* **110**, 9914–9919 (2013).
60. D. Pan, D. A. Hunter, L. Schellhardt, A. Fuchs, A. E. Halevi, A. K. Snyder-Warwick, S. E. Mackinnon, M. D. Wood, T cells modulate IL-4 expression by eosinophil recruitment within decellularized scaffolds to repair nerve defects. *Acta Biomater.* **112**, 149–163 (2020).
61. S. González-Medina, Equine eosinophilic keratitis: An emergent ocular condition? *Equine Vet. Educ.* **31**, 609–616 (2019).
62. J. Benitez-Del-Castillo Sánchez, M. D. Morillo-Rojas, C. Galbis-Estrada, M. D. Pinazo-Duran, Determination of inmune response and inflammation mediators in tears: Changes in dry eye and glaucoma as compared to healthy controls. *Arch. Soc. Esp. Oftalmol.* **92**, 210–217 (2017).
63. E. A. Jacobsen, K. R. Zellner, D. Colbert, N. A. Lee, J. J. Lee, Eosinophils regulate dendritic cells and Th2 pulmonary immune responses following allergen provocation. *J. Immunol.* **187**, 6059–6068 (2011).
64. L. Chen, K. A. Grabowski, J. P. Xin, J. Coleman, Z. Huang, B. Espiritu, S. Alkan, H. B. Xie, Y. Zhu, F. A. White, J. Clancy Jr., H. Huang, IL-4 induces differentiation and expansion of Th2 cytokine-producing eosinophils. *J. Immunol.* **172**, 2059–2066 (2004).
65. P. F. Weller, L. A. Spencer, Functions of tissue-resident eosinophils. *Nat. Rev. Immunol.* **17**, 746–760 (2017).
66. M. A. Stepp, J. D. Zieske, V. Trinkaus-Randall, B. M. Kyne, S. Pal-Ghosh, G. Tadvalkar, A. Pajoohesh-Ganji, Wounding the cornea to learn how it heals. *Exp. Eye Res.* **121**, 178–193 (2014).
67. E. A. Susaki, K. Tainaka, D. Perrin, H. Yukinaga, A. Kuno, H. R. Ueda, Advanced CUBIC protocols for whole-brain and whole-body clearing and imaging. *Nat. Protoc.* **10**, 1709–1727 (2015).

Acknowledgments

Funding: This research was supported by the National Eye Institute grants R01EY029055 (JHE), the Morton Goldberg Professorship (JHE), the NIH Directors Pioneer Award, a sponsored research agreement with ACell Inc., and the Intramural Research Program of the NIH, National Cancer Institute, CCR, and LCIM. We would also like to acknowledge EY001765 Wilmer Core Grant for Vision Research, the National Science Foundation's support (DGE-1746891) for D.R.M, and the NIH T32 Translational Aging Research Training Fellowship and an NIH T32 Nanotechnology for Cancer Research Fellowship for J.I.A. **Author contributions:** X.W. and L.C.: Design and execution of all experiments, manuscript preparation, and revision; J.H. and D.R.M.: Animal surgeries and experiments and flow cytometry; A.L.: Flow cytometry and manuscript revision; J.I.A.: NanoString and flow cytometry; A.F.C. and M.W.: Light sheet microscopy imaging; L.H. and N.T.R.: Material preparation and characterization; M.A.S.: Animal model advisor; F.H.: Immunology advisor; and J.H.E.: Design and supervision of all experiments, manuscript preparation, and revision. **Competing interests:** This study is a discussion of off-label use of UBM devices, which have not been cleared by the FDA for these indications. L.H. and N.T.R. are employees and shareholders of ACell Inc. J.H.E., X.W., and L.C. are inventors on a patent application related to this work filed by Johns Hopkins University (no. 63/047,219, filed 01 July 2020). The authors declare that they have no other competing interests. **Data and materials availability:** All data needed to evaluate the conclusions in the paper are present in the paper and/or the Supplementary Materials. Additional data related to this paper may be requested from the authors. The material transfer agreement (MTA) can be provided by the corresponding author pending scientific review. Requests for the MTA should be submitted to: jhe@jhu.edu.

Submitted 10 August 2020
Accepted 3 March 2021
Published 16 April 2021
10.1126/sciadv.abe2635

Citation: X. Wang, L. Chung, J. Hooks, D. R. Maestas Jr., A. Lebid, J. I. Andorko, L. Huleihel, A. F. Chin, M. Wolf, N. T. Remlinger, M. A. Stepp, F. Housseau, J. H. Elisseeff, Type 2 immunity induced by bladder extracellular matrix enhances corneal wound healing. *Sci. Adv.* **7**, eabe2635 (2021).